Numerical prediction of peri-implant bone adaptation: Comparison of mechanical stimuli and sensitivity to modeling parameters

Piccinini, Marco; Cugnoni, Joël; Botsis, John; Ammann, Patrick; Wiskott, Anselm

How to cite

PICCININI, Marco et al. Numerical prediction of peri-implant bone adaptation: Comparison of mechanical stimuli and sensitivity to modeling parameters. In: Medical engineering & physics, 2016, vol. 38, n° 11, p. 1348–1359. doi: 10.1016/j.medengphy.2016.08.008

This publication URL: https://archive-ouverte.unige.ch//unige:89035
Publication DOI: 10.1016/j.medengphy.2016.08.008

Medical Engineering and Physics 38 (2016) 1348–1359

Contents lists available at ScienceDirect

Medical Engineering and Physics

journal homepage: www.elsevier.com/locate/medengphy

Numerical prediction of peri-implant bone adaptation: Comparison of mechanical stimuli and sensitivity to modeling parameters

Marco Piccinini[a], Joel Cugnoni[a,*], John Botsis[a], Patrick Ammann[b], Anselm Wiskott[c]

[a] Laboratory of Applied Mechanics and Reliability Analysis, École Polytechnique Fédérale de Lausanne, Station 9, CH-1015 Lausanne, Switzerland
[b] Division of Bone Diseases, Department of Internal Medicine Specialities, Geneva University Hospitals and Faculty of Medicine, CH-1205 Geneva, Switzerland
[c] Division of Fixed Prosthodontics and Biomaterials, School of Dental Medicine, University of Geneva, CH-1211 Geneva, Switzerland

ARTICLE INFO

Article history:
Received 29 January 2015
Revised 5 August 2016
Accepted 30 August 2016

Keywords:
Bone adaptation
Implants integration
Overloading
Specimen-specific
Finite element
Gait
Mechanical stimulus

ABSTRACT

Long term durability of osseointegrated implants depends on bone adaptation to stress and strain occurring in proximity of the prosthesis. Mechanical overloading, as well as disuse, may reduce the stability of implants by provoking bone resorption. However, an appropriate mechanical environment can improve integration. Several studies have focused on the definition of numerical methods to predict bone peri-implant adaptation to the mechanical environment. Existing adaptation models differ notably in the type of mechanical variable adopted as stimulus but also in the bounds and shape of the adaptation rate equation. However, a general comparison of the different approaches on a common benchmark case is still missing and general guidelines to determine physically sound parameters still need to be developed. This current work addresses these themes in two steps. Firstly, the histograms of effective stress, strain and strain energy density are compared for rat tibiae in physiological (homeostatic) conditions. According to the Mechanostat, the ideal stimulus should present a clearly defined, position and tissue invariant lazy zone in homeostatic conditions. Our results highlight that only the octahedral shear strain presents this characteristic and can thus be considered the optimal choice for implementation of a continuum level bone adaptation model. Secondly, critical modeling parameters such as lazy zone bounds, type of rate equation and bone overloading response are classified depending on their influence on the numerical predictions of bone adaptation. Guidelines are proposed to establish the dominant model parameters based on experimental and simulated data.

1. Introduction

The process of bone adaptation to mechanical stimulations is often modeled at the continuum scale through the Mechanostat [1]. This theory postulates that a specific mechanical stimulus occurring in bone is kept within a physiological range (i.e. the lazy zone, LZ) through the variation of bone mass [2,3] which in turns affect the distribution of elastic modulus in the bone structure. These phenomenological adaptation models represent at the continuum scale the net result of the local bone adaptation process: the sensor network formed by osteocytes and their complex signaling is described by a mechanical measure of the stress and strain in a control volume (the "stimulus") while the activity of the osteoblasts and osteoclasts resulting in different rates of local bone apposition and resorption are represented by the rate of change of bone density at the continuum scale (the "bone apposition rate"). In extreme conditions, when bone is overloaded, continuous damage accumulation supersedes the capacity of bone to adapt and repair itself, which is represented in the adaptation models by a fast reduction of bone stiffness and/or mass above a certain overloading threshold. Several adaptation models have been implemented in order to evaluate the integration of implants, for example in dentistry [4–6] by considering both bone apposition and resorption due to overloading. The interplay between these phenomena has been seen to regulate the peri-implant marginal loss and determine the long term stability of dental implants [7,8].

Despite their versatility, these phenomenological approaches rely on many assumptions that are difficult to verify by experimentation and rarely discussed [9], such as: the choice of a mechanical signal which drives the bone adaptation ('stimulus'), the relation between the bone adaptation rate and the stimulus, the limits of bone adaptation and the size of the zone of stimulus diffusion in non-local models.

Indeed, the first open question concerns the choice of the mechanical variable used as a triggering signal. Investigations

* Corresponding author. Fax: +41 21 693 73 40.
E-mail addresses: marco.piccinini@epfl.ch (M. Piccinini), joel.cugnoni@epfl.ch (J. Cugnoni), john.botsis@epfl.ch (J. Botsis), Patrick.Ammann@hcuge.ch (P. Ammann), Anselm.Wiskott@unige.ch (A. Wiskott).

http://dx.doi.org/10.1016/j.medengphy.2016.08.008
1350-4533/

studying signals based on strain [1,10], strain energy density [2] or stress [11,12] all lead to satisfying results in specific applications when properly calibrated, however, there is no clear agreement on which regulation signal provides the best consistency in a general sense. Moreover, signal selection and the definition of bone apposition and resorption thresholds are not frequently discussed and comparisons are rare [5,13].

The mathematical form of the adaptation law which relates the level of mechanical stimulus to the bone apposition or resorption rate is also an open question. In order to preserve the natural structure of bone under physiological conditions, continuum level isotropic bone adaptation models must at least exhibit a region of homeostasis by defining a so-called lazy zone (LZ). The LZ represent an equilibrium condition at which normal bone turnover occurs, i.e. the resorption rate controlled by osteoclasts is equal to the apposition rate due to osteoblasts activity. The limits of the LZ and the bone overloading threshold are critical variables that control the adaptation process by governing the transition between bone resorption, homeostasis , apposition and damage. However, because of their potential dependency on species, location and biovariability, those bounds are difficult to determine and are only rarely defined on a rigorous experimental basis [14]. Furthermore, the dependence of bone adaptation rate on the mechanical stimulus has been formulated through linear [15], quadratic [16] or piecewise functions including a rate saturation [17], but the sensitivity of the obtained predictions to these different mathematical forms remains unclear.

Since bone adaptation is assumed to be driven by cell mechanotransduction [18], several adaptation models involve a spatial averaging of the stimulus over a zone of influence (ZOI) [3,19,20] to represent diffusion processes. The size of the ZOI affects the accuracy of numerical predictions but this dependence is scarcely investigated.

Furthermore, the pre-implantation bone structure and geometry differs significantly among one group of individuals, which limits the validity of predictions based on an average representative geometry. Biovariability is expected to induce a significant scatter in results of bone adaptation and this point is seldom discussed.

This work aims at establishing guidelines for the definition of the hypothesis needed to obtain accurate predictions of bone adaptation around implants. The modeling parameters, adaptation theories and mechanical stimuli are classified as critical, important or negligible with respect to their influence on results and methods are proposed to choose the values of the dominant parameters. The 'loaded implant' animal model is adopted as a benchmark [21]. This animal model allows investigating the effects of a controlled external stimulation of the bone tissue surrounding two transcutaneous implants inserted in the proximal part of rats' tibiae [22,23]. The 'loaded implant' model was chosen here as it allows a precise control of the loading history and implant placement but also because it closely mimics the difficulties found in clinical implantations in which a complex three dimensional stress state with local stress concentrators are commonly observed. Different mechanical stimuli are compared on the benchmark of full tibiae being subjected to physiological loading conditions. Assuming that the Mechanostat hypothesis is valid, a clear lazy zone should be able to be observed in the distribution of proper adaptation mechanical stimuli under such conditions. Moreover, the LZ of the ideal mechanical stimulus should also satisfy the criteria of location independence, tissue independence and specimen independence. The stimulus which best satisfies these conditions is identified and used in combination with a specimen-specific adaptation algorithm to predict bone peri-implant adaptation. A sensitivity study subsequently highlights the dependence of bone adaptation results on the LZ, on the adaptation law, on the ZOI, on the load level and on biovariability.

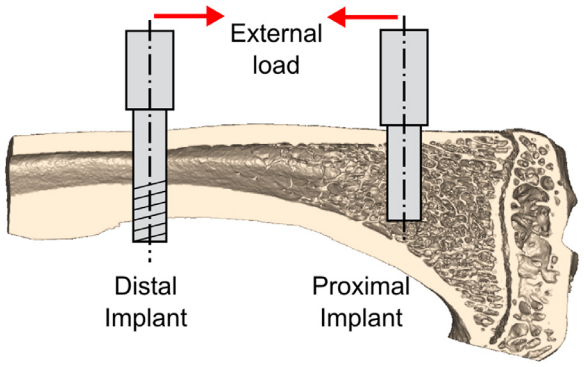

Fig. 1. Working principle of the 'loaded implant' model: two titanium implants are screwed mono and bi-cortically into the proximal part of the rat tibia (view cut). A controlled stimulation is provided daily by pulling the implants heads together.

2. Materials and methods

2.1. Animal model

Two transcutaneous Ti implants were screwed mono- and bicortically into the right tibia of female Sprague-Dawley rats (Fig. 1) following the procedures described in [22,23]. After two weeks of integration, five animals were euthanized. This 'basal' group represented the pre-stimulation integration state of the 'loaded implant' model and was used as a basis for bone adaptation simulation. The remaining animals ('stimulated group') were subjected to a controlled external load of 5 N, applied on a daily basis to force the implant's heads together and to stimulate the bone tissue around them. The load was applied with the following schedule: 1 Hz sinusoidal cycle from 0 N to 5 N, 900 cycles/day, 5 days/week for 4 weeks (total of 20 days of stimulation) with a progressive increase of load amplitude during the first week (+1 N/day). After sacrifice, all tibiae were dissected, cleared of their soft tissue coverage and frozen at −21 °C. The specimens were then thawed out and analyzed using a high resolution CT imaging system (μCT-40, Scanco Medical AG, Brüttisellen, Switzerland, isotropic voxel size: 20 μm). The technical aspects of surgery, implant design, activation setup and CT imaging that characterize the 'loaded implant' model are described in detail in [22–24].

2.2. Finite element models

Continuum-level specimen-specific FE models of bare and implanted rat tibiae were generated from CT scans through a verified and validated procedure [24]. The CT images were segmented to isolate the continuum bone and implants domains and processed with an open-source FE model generator to quality second order tetrahedral meshes. These models represent the whole bone structure as a continuum, elastic, isotropic and inhomogeneous material. The local average BMD is calculated in each element of the model using the mean BMD of the CT voxels contained in the elements. To avoid potential checkerboard patterns and oscillations, the BMD field is then averaged at the nodes of the mesh to obtain a continuous description. Subsequently, the integration points were assigned their material properties by interpolation of the nodal BMD and by using the density-elasticity relationship developed by Cory et al. [25]. Five whole tibiae were processed to generate specimen-specific FE models, which were then subjected to a gait-based loading condition that had been shown to generate a sound physiological pattern of deformation [26] (Fig. 2a). These specimens were adopted as the benchmark for the comparison of mechanical stimuli.

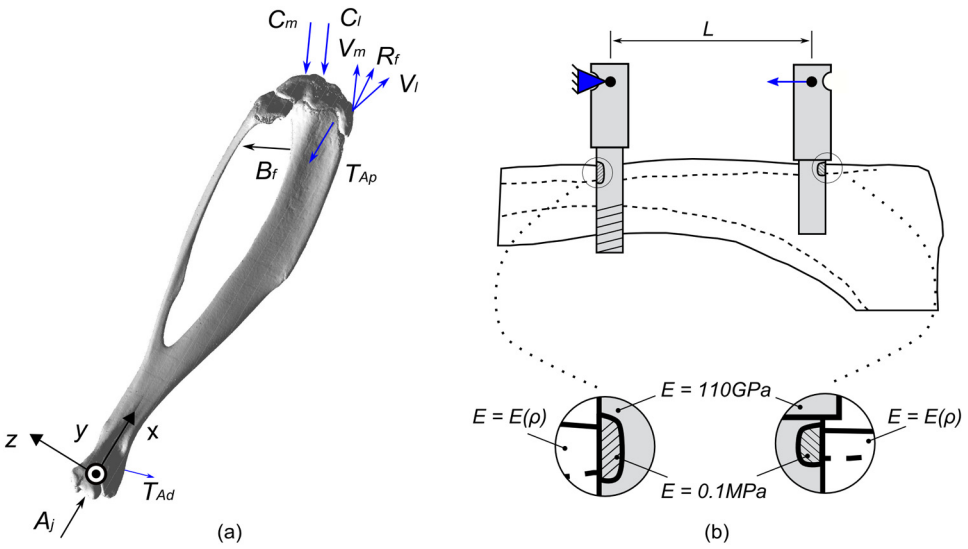

Fig. 2. (a) Gait-based loading condition applied to FE models of whole tibiae for the comparison of stimuli [26]. Loads: medial and lateral condylar reactions, C_m and C_l, ankle joint reaction A_j, bicep femoris B_f, vastus medialis V_m and lateralis V_l, rectus femoris R_f, tibialis anterior proximal T_{Ap} and distal T_{Ad}. (b) Loading condition applied to FE models of implanted specimens for iterative computations. The dotted areas are characterized by a small elastic modulus. L is the inter-implant distance.

Five implanted specimens scanned at the 'basal' state were processed in order to generate the FE models for iterative computations on bone peri-implant adaptation. These specimens represented the pre-stimulation integration state of the 'loaded implant' model: they underwent two weeks of post-surgery integration which allowed the primary stability to be established [22], but no external loading. These FE models were subjected to the boundary conditions shown in Fig. 2b corresponding to the controlled loading provided during in-vivo stimulation. The bone-implant contact was considered perfectly adherent. However, in order to prevent unrealistic transfer of loads to the tissue where the interface was subjected to traction [26], a small elastic modulus was assigned to a narrow strip of the tensile loaded regions of the implants in contact with cortical bone in the distal and proximal directions.

2.3. Mechanical stimuli

Based on the hypothesis of the Mechanostat and Wolff's law, an appropriate continuum 'stimulus' variable should exhibit a clear lazy zone in homeostatic conditions i.e. values of the stimulus variables should be strictly bounded in homeostatic conditions. To have an objective bone adaptation model, the LZ of the stimulus should also be independent on the location within bone, if possible also independent on the tissue type and ideally be as homogeneous as possible among a population. So, formally, an adequate stimulus variable should respect the following criteria under physiological homeostatic conditions:

- *Location invariance*. Under homeostatic conditions, different regions of the same bone should show the same range of stimulus (i.e. the same width of the histogram of stimulus in different regions).
- *Tissue invariance*. Ideally, the 'stimulus' variable should be independent on the bone structure. Thus cortical and trabecular bone should show the same stimulus range as well (i.e. the same width of the histogram of stimulus in both tissues).
- *Specimen invariance*. The histogram of the stimulus should be homogeneous within a population of specimens.

If these conditions are not satisfied, the bone adaptation process would become site-specific [10] meaning that the bone cells should know a priori their position in the tissue and their target equilibrium condition.

Three isotropic scalar stimuli were compared by highlighting their compatibility with these criteria, on the benchmark of whole tibiae subjected to physiological deformations [26].

The first stimulus considered was the elastic energy per unit of mass ψ_U (Eq. (1)) [10,16]. This energy-based stimulus combines the continuum level strain energy density U_i that occurs during the loading condition i, the local apparent bone density ρ, and the number of loading conditions N.

$$\psi_U = \frac{1}{N}\sum_{i=1}^{N}\frac{U_i}{\rho} \tag{1}$$

As described by Weinans et al. [10], ψ_U represents the average local strain energy density in the trabeculae over a series of loading cycles and thus is a global measure of the intensity of the local mechanical environment perceived, directly or indirectly, by the osteocytes.

The second stimulus considered was daily stress ψ_σ (Eq. (2)) [11,12], formulated as

$$\psi_\sigma = \left(\frac{\rho_c}{\rho}\right)^2 \cdot \left(\sum_{i=1}^{N} n_i \sigma_i^m\right)^{1/m} \tag{2}$$

ρ_c is the apparent density of mineralized bone and m is an empirical constant adopted to weigh the number of cycles and stress depending on the physical activity. This stimulus depends on multiple load cases N, on the number of loading cycles n_i and on the effective stress at the continuum level σ. As described by Beaupré et al. [11] , ψ_σ represents the daily average stress at the trabeculae level (hence the factor $(\frac{\rho_c}{\rho})^2$) and is indirectly related to the strain energy measure ψ_U through the elastic modulus of bone.

The third stimulus considered was the octahedral shear strain. Frost introduced the hypothesis that the Mechanostat is driven by the peak daily strains that occur in the bone tissue [1]. Since shear has been shown to influence tissue differentiation [27,28], the strain-based stimulus ψ_ε was formulated as a function of the octahedral shear strain ε_{oct}:

$$\psi_\varepsilon = \max(\varepsilon_{oct,1}, \varepsilon_{oct,2} \ldots, \varepsilon_{oct,N}) \text{ with}$$
$$\varepsilon_{oct} = \frac{2}{3}\sqrt{(\varepsilon_1-\varepsilon_2)^2 + (\varepsilon_2-\varepsilon_3)^2 + (\varepsilon_3-\varepsilon_1)^{2\ldots}} \tag{4}$$

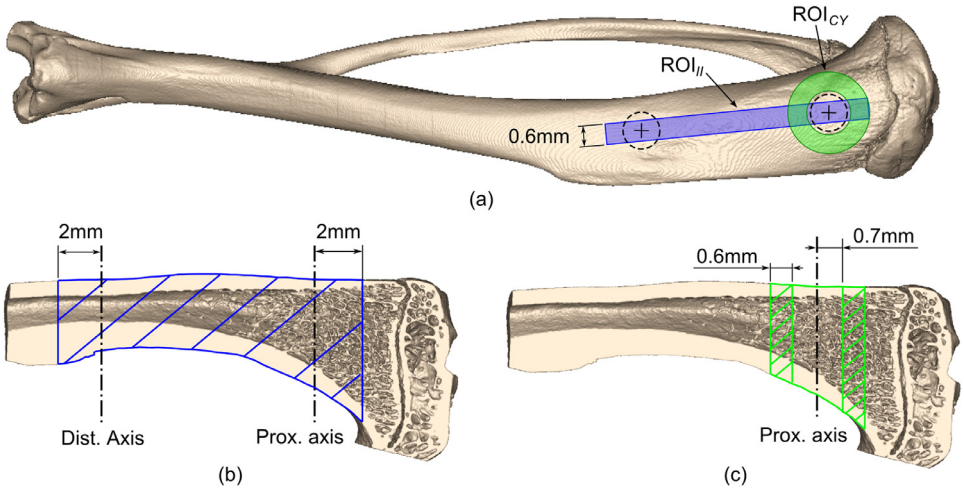

Fig. 3. ROIs for the comparison of mechanical stimuli. (a) Positioning of the inter-implant and cylindrical regions of interest with respect to the implants insertion coordinates (ROI_{II} and ROI_{CY}, respectively). View cuts of the tibia: overall dimensions of (b) ROI_{II} and (c) ROI_{CY}.

in which ε_i denotes the ith principal value of the continuum strain tensor $\boldsymbol{\varepsilon}$. In the case of a lattice of straight trabeculae in tension or compression, the stimulus ψ_ε represents also the local strain experienced in the bone tissue. The three signals are investigated through a single loading condition ($N = i = 1$), based on the peak musculoskeletal loads occurring during gait [26]. The number of loading cycles characterizing daily stress was fixed to $n = 1$. As a consequence, the considered energy, stress and strain-based stimuli are formulated as shown in Eqs. (5)–(7), respectively.

$$\psi_U = \frac{U}{\rho_{bmd}} \tag{5}$$

$$\psi_\sigma = \left(\frac{\rho_{bmd,c}}{\rho_{bmd}}\right)^2 \cdot \sigma \tag{6}$$

$$\psi_\varepsilon = \varepsilon_{oct} \tag{7}$$

where ρ_{bmd} and $\rho_{bmd,c}$ are the local and the fully mineralized BMD (i.e. 1.2 gHA/cm^3).

The stimuli distribution was investigated in two fixed regions of interest (ROI) with respect to the location of the implants (Fig. 3a). The region ROI_{II} was obtained by a dilatation of +/− 0.3 mm of the plane where both implant axes lie. ROI_{II} represented the region where the external stimulation was more effective. The region ROI_{CY} was defined as a cylinder surrounding the proximal implant location. It provided an estimation of stimulus around the floating implant. Overall dimensions can be seen in Fig. 3b and c.

To analyze tissue invariance, the signals were also differentiated between cortex, trabecular tissue and marrow through BMD thresholds. In detail, stimuli were classified as cortical if BMD > 0.8 gHA/cm^3, and trabecular if $0.3 <$ BMD < 0.8 gHA/cm^3 [25]. These BMD thresholds approximately corresponded to BV/TV values of 0.25 and 0.6 respectively. Results belonging to "marrow" (BMD < 0.3 gHA/cm^3) were neglected. For each ROI, tissue category and specimen, the volume histogram of the investigated stimulus variable was reconstructed from the FE simulation results. The mean value and SEM of the histograms of five specimens were finally calculated and compared in order to evaluate the aforementioned invariance criteria.

2.4. Bone adaptation algorithm

The simulations of bone adaptation were based on the hypothesis that the mechanical stimulus tends towards a constant range of values, corresponding to the LZ [1,11], by reducing or increasing the bone density. The density variation was computed through the formulation described in Eq. (8), inspired by Li et al. [16]:

$$\frac{d\rho_{bmd}}{dt} = \begin{cases} 0 & if \quad \psi \le \psi_a \\ K_a(\psi - \psi_a)\left(1 - \frac{\psi - \psi_a}{\psi_d - \psi_a}\right) & if \quad \psi > \psi_a \end{cases} \tag{8}$$

where ψ is the chosen mechanical stimulus, K_a is the adaptation rate, and ψ_d and ψ_a are the damage and apposition LZ limits, respectively (Fig. 4a). This formula implies that implant loading has no effect if the stimulus is low ($d\rho_{bmd}/dt = 0$ if $\psi < \psi_a$), a positive effect of the stimulation if the stimulus is in the apposition range ($d\rho_{bmd}/dt > 0$ if $\psi_a < \psi < \psi_d$) and resorption due to overloading occurs if the stimulus overcomes the damage limit ($d\rho_{bmd}/dt < 0$ if $\psi > \psi_d$). Disuse was not considered as physiological loads were sufficient to maintain the bone structure [16,17]. This formulation implies a parabolic evolution of the apposition rate with a maximum at a stimulus $\psi = \frac{1}{2}(\psi_a + \psi_d)$ followed by a progressive reduction representing sub critical damage accumulation in the bone up to $\psi = \psi_d$ where bone damage accumulation cannot be compensated any more.

The calculation of the effective stimulus included a spatial averaging of the mechanical variables over a spherical zone of influence (ZOI) [3] which represents the diffusion distance associated to mechanotransduction signaling. In detail, the signal at each node was calculated through Eq. (9)

$$\psi_i = \frac{\psi_i + \sum_{j=1}^{Z} f(D_{ji})\psi_j}{1 + \sum_{j=1}^{Z} f(D_{ji})} \tag{9}$$

Z is the number of nodes included in the defined ZOI and $f(D_{ji})$ is a function that weighs the signal contribution of the node j with respect to its distance D_{ji} from the current node i.

Eq. (8) was solved iteratively through forward Euler integration in order to update bone density in relation to tissue deformation until convergence. A controlled BMD variation was calculated at each iteration with an adaptive time step to guarantee the stability of the simulations [29].

2.5. Sensitivity analyses

Five specimen-specific FE models of implanted tibiae were processed with different sets of parameters to perform a sensitivity study on the numerical predictions of bone adaptation. Due to the large number of parameters, the study was structured into several

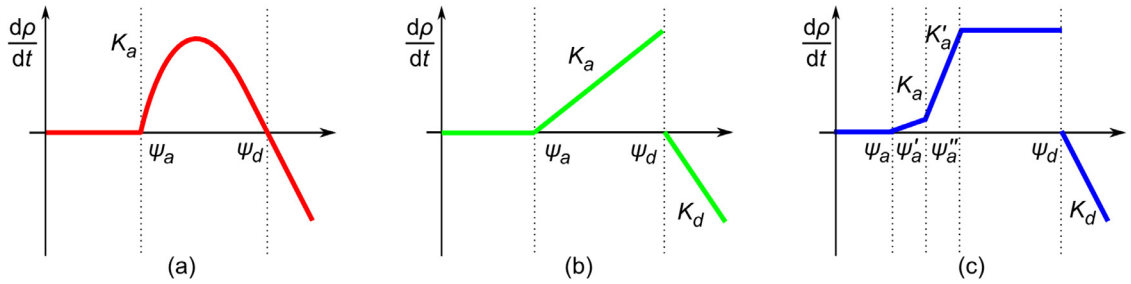

Fig. 4. Adaptation rate $d\rho/dt$ versus mechanical stimulus ψ (a) quadratic form (b) linear form and (c) piecewise form with plateau.

Table 1
Details of sensitivity studies.

Parameter		Nominal	Levels	# simulations
Adaptation thresholds ($\cdot 10^{-2}$)	ψ_a	1.25	1; 1.25; 1.5; 1.75	80
	ψ_d	4.51	4.1; 4.51; 1.5; 5.5	
ZOI	Radius (mm)	0.3	0; 0.15; 0.3; 0.6; 0.9	65
	Type	Gaussian	Linear, Gaussian, exponential	
Law formulation		Quadratic	Linear, quadratic, plateau	15
External load (N)		5	3.3; 5; 6.7; 8.3; 10	25

separate parametric studies, which are presented in the following sections and summarized in Table 1.

2.5.1. Nominal parameters

Based on the invariance analysis of the mechanical variables (Section 3.1), the octahedral strain stimulus was chosen as the reference signal for the sensitivity analysis. The correlation between mechanical stimulus and bone apposition rate was provided by Eq. (8), and the value of the apposition threshold, $\psi_a = 1.25 \times 10^{-3}$, was fixed in agreement with the physiological deformations occurring in rat tibiae during gait [26]. The value of the damage threshold $\psi_d = 4.51 \times 10^{-3}$ was fixed in agreement with the longitudinal strain limit of 4×10^{-3} already adopted for a study concerning bone damage [15]. As the steady state solution was only of interest in the present study, the adaptation rate K_a was given the value of 1 (gHA/cm3)/(time unit) similarly to Li et al. [16]. The nominal ZOI radius was chosen corresponding to the limit of validity of continuum description ('LVC') of trabecular bone as described in [30], corresponding to 3–5 inter-trabecular lengths which is estimated at 0.3 mm in the present case. The decay of the signal with increasing distance from the central node of the ZOI was computed through a Gaussian function (Eq. (10)), which is typical for many diffusion-like natural processes [19].

$$f(D_{ji}) = e^{-\frac{D_{ji}/r}{2\beta^2}} \tag{10}$$

with $\beta = 0.4085$. These settings are considered as the reference for the sensitivity study.

2.5.2. Sensitivity to the lazy zone thresholds

The ranges of octahedral shear strain thresholds ψ_a and ψ_d were discretized in four intervals between 1×10^{-3} and 1.75×10^{-3}, and 4.1×10^{-3} and 5.5×10^{-3}, respectively. The bone adaptation solutions were computed for each specimen and each pair of adaptation thresholds, while keeping all other parameters at their nominal values therefore leading to 80 simulations.

2.5.3. Sensitivity to the adaptation law formulation

Three mathematical formulas of the adaptation law were compared: the quadratic form in Eq. (8), a linear formulation [15] and a piecewise law with a plateau [17] (Eq. (11) and Fig. 4b, Eq. (12) and Fig. 4c, respectively), for a total of 15 simulations.

Table 2
Parameters of the adaptation laws.

Law	Eqs.	Adaptation thresholds ($\cdot 10^{-2}$)				Rate constant		
		ψ_a	$\psi_a{}'$	$\psi_a{}''$	ψ_d	K_a	$K_a{}'$	K_d
Quadratic	(2)	1.25	–	–	4.51	1	–	–
Linear	(5)	1.25	–	–	4.51	1	–	1
Plateau	(6)	1.25	1.5	1.75	4.51	0.05	1	1

$$\frac{d\rho}{dt} = \begin{cases} 0 & if \quad \psi \le \psi_a \\ K_a(\psi - \psi_a) & if \quad \psi_a < \psi \le \psi_d \\ K_d(\psi - \psi_d) & if \quad \psi > \psi_d \end{cases} \tag{11}$$

$$\frac{d\rho}{dt} = \begin{cases} 0 & if \quad \psi \le \psi_a \\ K_a(\psi - \psi_a) & if \quad \psi_a < \psi \le \psi'_a \\ K_a(\psi'_a - \psi_a) + K'_a(\psi_a - \psi'_a) & if \quad \psi'_a < \psi \le \psi''_a \\ K_a(\psi'_a - \psi_a) + K'_a(\psi''_a - \psi'_a) & if \quad \psi''_a < \psi \le \psi_d \\ K_d(\psi - \psi_d) & if \quad \psi_d < \psi \end{cases} \tag{12}$$

The adopted parameters were calculated to preserve the nominal adaptation thresholds and are presented in Table 2. Compared to the quadratic form in Eq. (8) which shows a peak apposition rate at $\psi = 2.88\%$, the linear adaptation model shows a maximum apposition rate at the bone damage threshold $\psi_d = 4.51\%$ followed by an abrupt transition to damage driven bone resorption. In contrast, the piecewise model in Eq. (12) presents a wide range of constant apposition rate which reaches its maximum rate (saturation) much earlier ($\psi''_a = 1.75\%$) than the other two models.

2.5.4. Sensitivity to the zone of influence

The ZOI radius r was varied from 0 to 0.9 mm, and three types of weight functions were considered: Gaussian, linear and exponential (Eqs. (10), (13) and (14)), for a total of 65 simulations.

$$f(D_{ij}) = 0.95\left(1 - \frac{D_{ij}}{r}\right) + 0.05 \tag{13}$$

$$f(D_{ij}) = e^{-2.99\frac{D_{ij}}{r}} \tag{14}$$

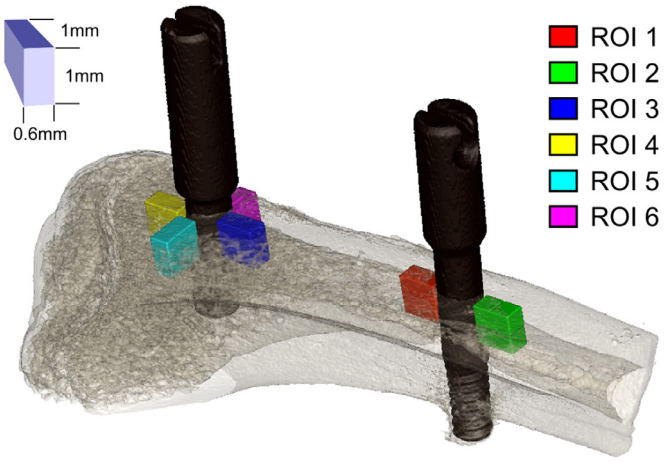

Fig. 5. Regions of interests (ROIs) where BMD is monitored.

To achieve comparable effects, the constants used in the different forms of $f(D_{ij})$ were chosen to achieve $f(D_{ij})=1$ for $D_{ij}=0$ and $f(D_{ij})=0.05$ for $D_{ij}=r$. The contribution of nodes outside the ZOI ($D_{ij} > r$) was neglected.

2.5.5. Sensitivity to load level

The specimen-specific FE models were simulated with default parameters at five applied load levels ranging from 3.3 to 10 N, therefore giving 25 simulations.

2.5.6. Convergence criteria and selected output variables

Simulations were stopped when 99.9% of nodes showed null adaptation errors (signal within lazy zone). Local BMD variations were assessed in six ROIs (Fig. 5). The longitudinal stability of implants was monitored by estimating the variation of inter-implant strain defined as d/L, where d and L are the relative inter-implant heads displacement and inter-implant distance, respectively.

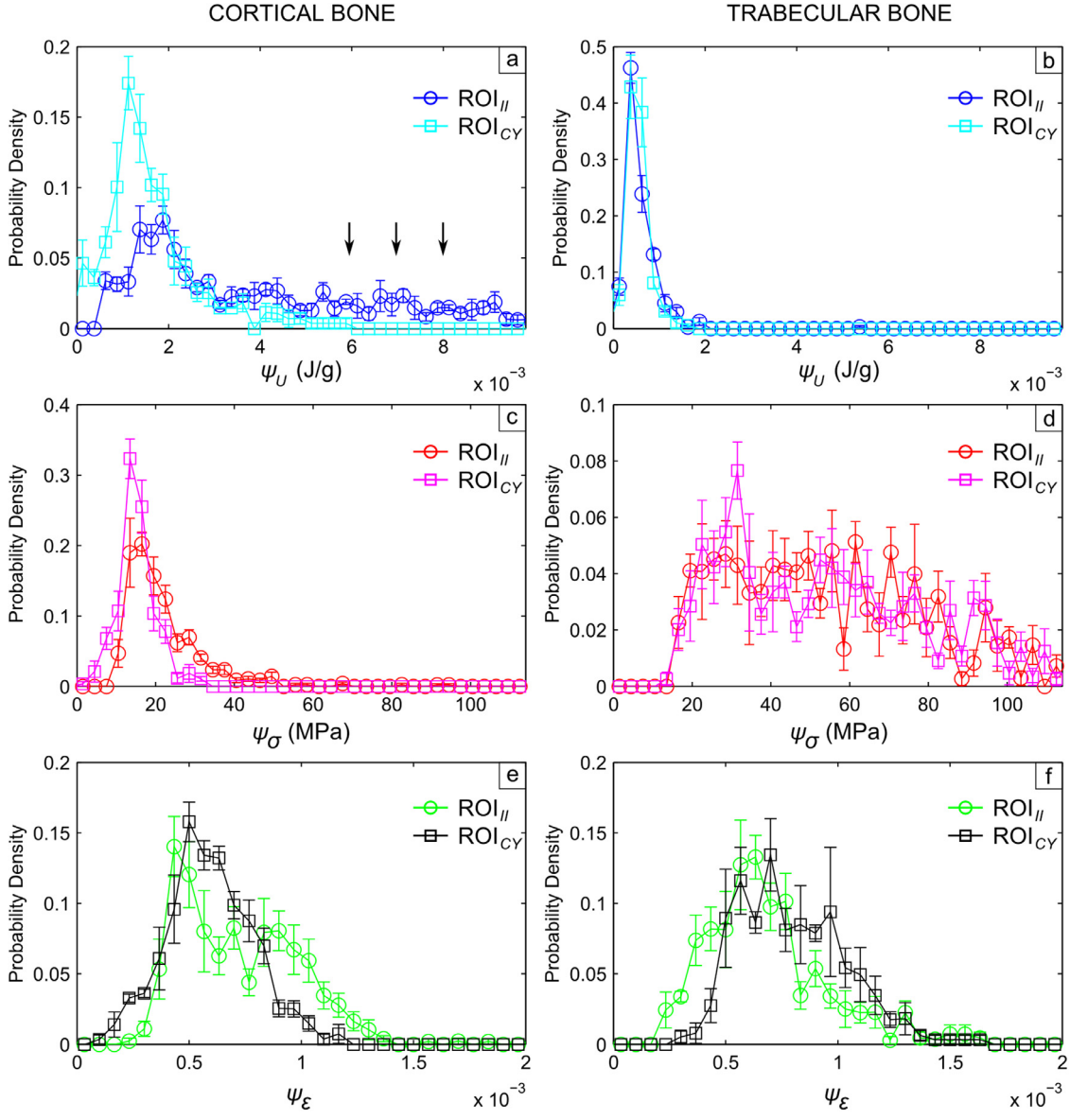

Fig. 6. Distribution of signals (rows) with respect to the tissue type (columns) and the regions of interest ROI_{II} and ROI_{CY} (legend). In detail: energy-based signal ψ_U in cortical (a) and trabecular (b) tissue, stress-based signal ψ_σ in cortical (c) and trabecular (d) tissue, and strain-based signal ψ_ε in cortical (e) and trabecular (f) tissue.

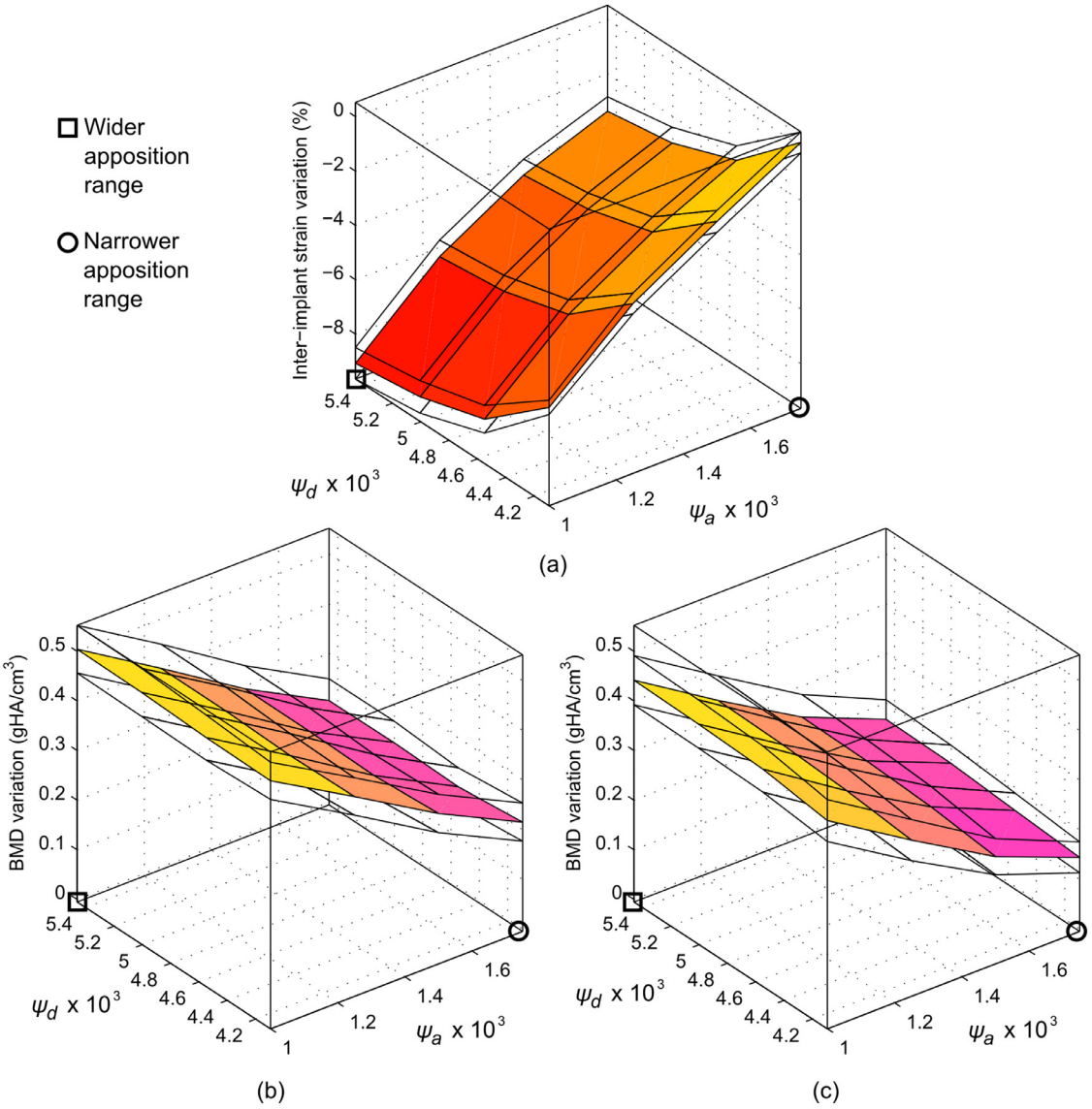

Fig. 7. Sensitivity of (a) inter-implant strain and BMD in (b) ROI1 and (c) ROI3 with respect to the perturbation of the apposition and damage thresholds (ψ_a and ψ_d). The mean values (colored surface) and the SEM (upper and lower grids) of the group of five specimens adopted as benchmark are represented.

3. Results

3.1. Comparison of stimuli

The histogram distributions of the signals belonging to different ROIs and tissues are shown in Fig. 6. Each distribution is represented by the mean ± SEM calculated on the five specimen-specific FE models of whole tibiae subjected to the gait-based loading condition [26]. Considering the energy-based stimulus ψ_U, a large amount of cortical bone in ROI_{II} shows levels of strain energy significantly larger to the ones measured in ROI_{CY} (~40% of the total, black arrows in Fig. 6a). Overall, the distributions in both ROIs are significantly different. For the trabecular bone, the distributions of ψ_U are similar between ROIs (i.e. nearly superimposed histograms, Fig. 6b). However, the range covered by ψ_U in trabecular bone (from 0 and 2×10^{-3} J/g) and cortical bone (between 0 and 8×10^{-3} J/g) are very different. Thus, the energy-based signal does not satisfy both location and tissue-invariance criteria.

The stress based stimulus ψ_σ shows location-invariant distributions, as shown by the negligible differences between ROIs in Fig. 6c and d, respectively. Nevertheless, the distributions in cortical and trabecular bone are not comparable either in terms of shape or in terms of range. As a consequence, even though it satisfies the location invariance criterion within a tissue, the stress-based signal does not satisfy the tissue-invariance criterion.

Finally, the distributions of the strain based stimulus ψ_ε are shown in Fig. 6e and f. The shape of the distributions is found to be similar in both ROIs and tissues, and the bounds of the strain based stimulus ψ_ε remains homogeneous (between 200 and 1500 $\mu\varepsilon$). These results therefore demonstrate that the strain based stimulus ψ_ε respects both the tissue and the location-invariance criteria under physiological conditions (i.e. during gait), and for this reason this stimulus is chosen as reference for the sensitivity study of bone adaptation.

As a unique range of physiological strain stimulus can be identified, the histograms can be used to set the apposition threshold of the adaptation model in physiological conditions. Indeed, the reference value of the apposition threshold, $\psi_a = 1.25 \times 10^{-3}$, is quantified as the 95th percentile of the octahedral shear strain distribution characterizing both tissues and ROIs during physiological activity.

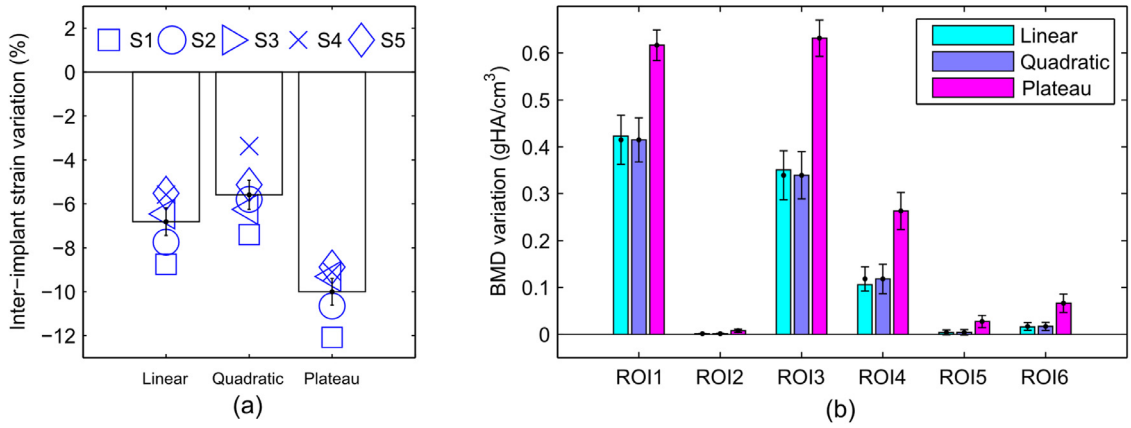

Fig. 8. Sensitivity of (a) inter-implant strain and (b) BMD in ROIs with respect to the law formulation. Mean values and SEM are represented.

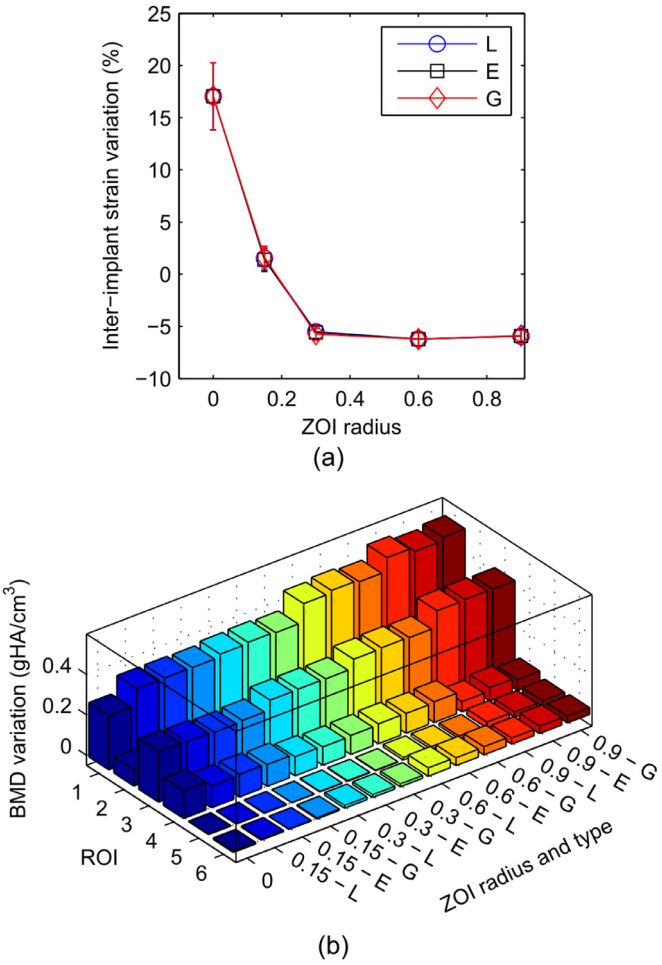

Fig. 9. Sensitivity of (a) inter-implant strain (mean values and SEM) and (b) BMD in ROIs with respect to the ZOI radius and weight function (i.e. L=linear, E=exponential, G=Gaussian).

3.2. Effect of adaptation thresholds

The results of this parametric study are shown in Fig. 7. The evolution of the inter-implant strain (inversely proportional to stiffness) varies between 0 and −8% with both ψ_a and ψ_d (Fig. 7a). The minimum and maximum increase of stiffness coincides with the wider and narrower amplitude of the apposition zone. Moreover, the effect of ψ_d reaches a plateau after 5×10^{-3}, meaning that the damage controlled adaptation is no longer activated above this point. At 5 N load, the value of the damage threshold ψ_d has a limited influence on inter-implant strain, which remains mostly controlled by the apposition threshold ψ_a. The BMD variation in ROI1 and ROI3 (Fig. 10b and c) shows an even clearer trend: the average BMD variation in different ROIs is nearly independent to ψ_d, whereas it is reduced with the increase of ψ_a.

3.3. Effect of adaptation law formulation

The effect of adaptation law formulation on inter-implant strain variation and BMD increment in ROIs are reported in Fig. 8a and b, respectively. Interestingly, the results of the quadratic and linear formulations show clear agreement, with the latter slightly underestimating the inter-implant strain and density increments with respect to the former. The mathematical form including a plateau involves a significant overestimation of both outputs. This highlights the fact that even though all three adaptation laws have similar thresholds, the shape of the adaptation law has an influence on the result.

3.4. Effect of the zone of influence

As shown in Fig. 9a, if the ZOI radius is lower than the limit of validity of the continuum assumption ('LVC', 3–5 inter-trabecular lengths) the inter-implant strain increases as the models predict a greater resorption due to overloading in regions close to the implant. The extreme case of no ZOI (r=0) provokes a 17% increase in inter-implant strain, which is the opposite of what is found with the nominal ZOI of 0.3 mm (−5.5%). For radii above the LVC, there is nearly no variation of the inter-implant strain, thus indicating that once the signal is averaged on a consistent volume of bone (i.e. compatible with the continuum hypothesis), the solution remains stable. The BMD variation shown in Fig. 9b shows a moderate increase in density with an increasing ZOI radius in ROI 1 and 2 both situated in the inter-implant plane, and subjected to compression. Interestingly, the effects of the different decay formulations are found to be negligible.

3.5. Effect of the load level

In Fig. 10, the inter-implant strain variation after convergence is plotted against the applied load for all five specimens (S1 to S5). A 3.3 N load provokes only a weak inter-implant strain reduction (−3%), which is then nearly doubled by imposing 5 N (−5.5%). With higher loads, the system stability decreases significantly and the effects of biovariability are strongly amplified. By applying

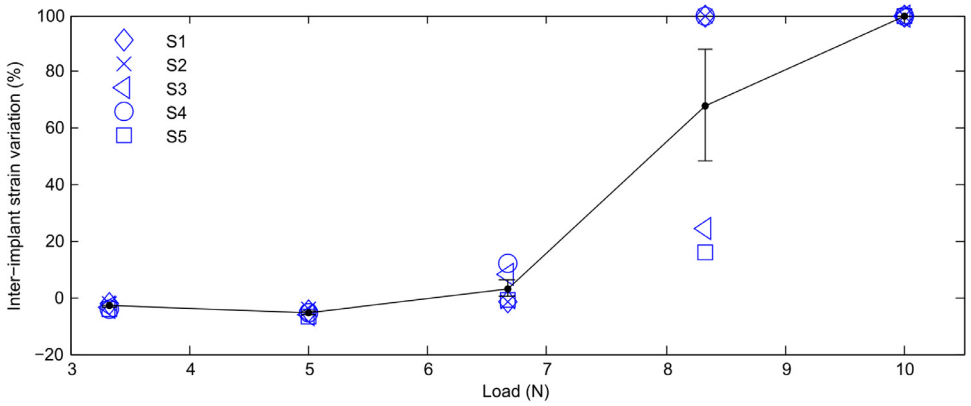

Fig. 10. Inter-implant strain sensitivity to the external load magnitude. Mean values and SEM are represented.

6.7 N, the average level of the inter-implant strain becomes positive (+3.3%, i.e. inter-implant stiffness decreases) with a larger spread with respect to lower load levels. At 8.6 N the imbalance between resorption and apposition reaches critical levels for 3 out of the 5 specimens, characterized by the failure of all the tissue surrounding the distal implant (Fig. 11). Nevertheless, two specimens did reach a stable converged solution with increased inter-implant strain (+20%). Finally, none of the FE models adapted to 10 N: resorption due to overloading dominates the adaptation mechanism provoking the instability of the distal implant. Inter-implant BMD fields estimated with all load levels are shown in Fig. 11.

The local BMD variations in the ROIs show a similar trend (Fig. 12) and explain the variations in implant stability. Indeed, at low force, increased BMD in the compressive regions between implants is correlated to the reduction of inter-implant strain. However, the average BMD in the ROIs continue to increase with higher loads (i.e. 6.3 and 8.7 N) but regions of significant bone resorption develop (Fig. 11), leading to a progressive reduction of the implant's stability. Thus, it is worth noticing that the implants stability and BMD variation in the selected ROIs are not correlated at high loads.

4. Discussion

This paper focuses on the reliability of Mechanostat-based predictions of bone adaptation estimated through specimen-specific, continuum FE models. The adopted modeling strategy relies on nominal parameters which are consistent with the physiology of the 'loaded implant' model and with the problem length-scale. The predictions obtained with these parameters were validated through comparison with in-vivo experiments and are used as reference [31]. Since these phenomenological predictions are the result of several assumptions, it is of great interest to clarify the methods which have been used to define the key parameters and highlight their influence on the results.

Three mechanical variables were compared on the benchmark of full tibiae subjected to physiological loading conditions. The analysis of the stimuli distribution (Fig. 6) with respect to position, tissue and specimen invariance criteria highlights that, among the three stimulus considered, the octahedral shear strain is the most appropriate stimulus for the implementation of the Mechanostat theory at the continuum scale. When physiological gait-based loads are applied, this signal is the only one that shows location, tissue and specimen-independent distributions as implied by the Mechanostat and Wolff's law. This result confirms the existence of a unique range of selected stimulus variable corresponding to physiological homeostatic conditions (i.e. the lazy zone), which drives bone macroscopic structural adaptation to mechanical stimulations. However, not all mechanical stimulus variable show this property.

An exhaustive sensitivity study highlighted the robustness of the adopted strategy by clarifying the influence of biovariability, bone adaptation thresholds, adaptation law formulation, ZOI and external load on numerical predictions. The effects of all these variables were evaluated by performing multiple specimen-specific iterative computations that generated results dependent on the features of each individual.

The default bounds of the lazy zone (i.e. apposition and damage thresholds ψ_a and ψ_d) were defined by analyzing physiological deformations occurring during rats' gait and reference literature data. Nevertheless, the dependency of results on the perturbation of these parameters is of great interest considering that the equilibrium between the peri-implant bone apposition and the apical resorption from overloading is a key factor in implant stability. The results show that the perturbation of the adaptation thresholds within consistent ranges of strain does not affect the robustness of the investigated adaptation process (e.g. no worsening of the implant lateral stability is predicted, Fig. 7). However, these parameters clearly affect the prediction of both BMD and inter-implant strain variations. This therefore highlights the need for a rigorous way of determining the apposition threshold ψ_a in particular. The determination of this parameter through an histogram analysis of the octahedral strain stimulus in physiological conditions, as used in this study, is highly recommended in order to obtain reliable predictions. Another possibility, however more complex and invasive, is obviously in-situ strain measurements under physiological conditions.

The mathematical formulation of the density adaptation rate dependence on the stimulus also has a strong influence on the results. The quadratic form adopted as reference (Eq. (8)) allows describing both apposition and resorption due to overloading with few parameters. This model also presents a smooth transition between apposition and damage-driven resorption. Nevertheless, this phenomenological formulation may not be representative of the actual correlation between bone mass variation and mechanical stimulus. In this work, the results obtained with the quadratic law are compared with the ones obtained with a linear form and a piecewise formulation which includes a plateau (Eqs. (11) and (12), respectively). The results shown in Fig. 8 highlight that the quadratic and linear formulations can be considered equivalent. On the contrary, the adoption of a formulation which includes a large plateau significantly affects the results, and lead to unrealistic predictions when compared to experimental observations [31, 32]. Thus, this type of formulation should only be implemented if the saturation of density rate is supported by a sound experimental validation.

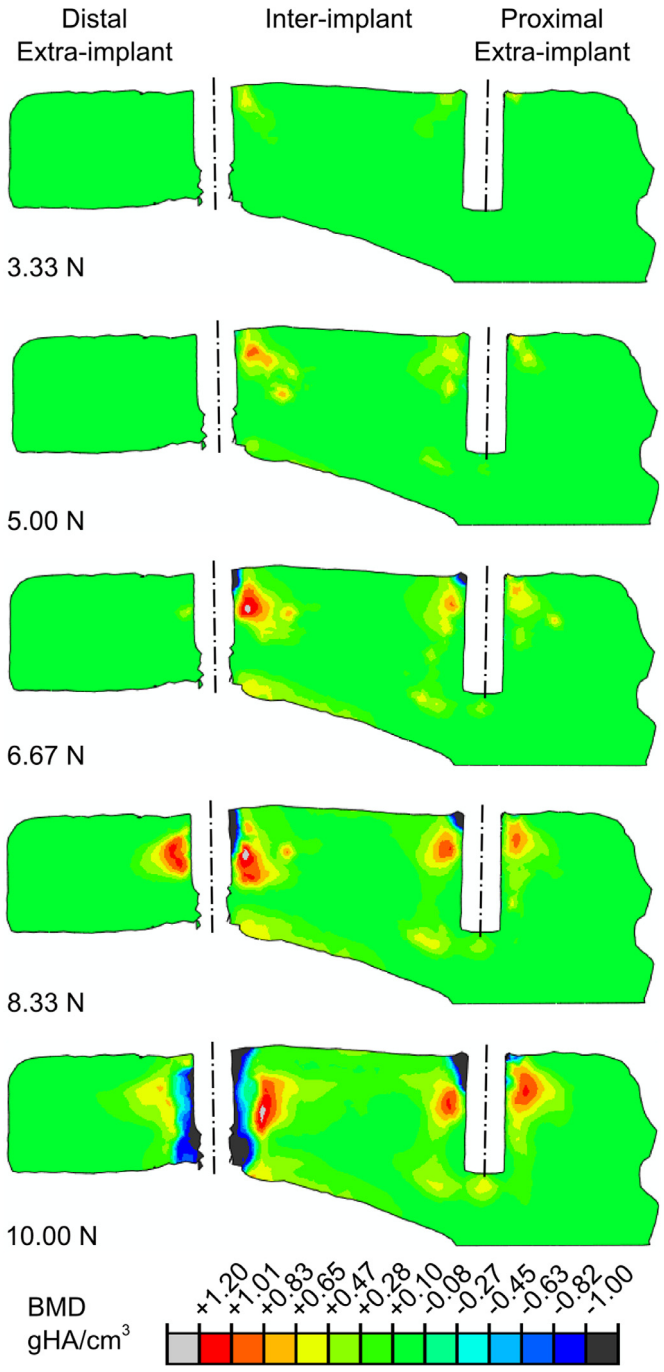

Fig. 11. BMD field variation with respect to the external load magnitude. Implants are hidden.

The stimulus average on a ZOI introduces the interesting concept of transmission of a local mechanical signal all around the stimulated area, via biological processes involving the tissue micro and cellular-structures. Moreover, the filtered stimulus is a measure of the mechanical state in a statistically representative volume of bone. It is thus of great interest to investigate the sensitivity of the numerical predictions to different ZOI dimensions and stimulus decay functions (Eqs. (10), (13) and (14)). The results of this study highlights that the definition of a ZOI is essential to predict consistent results (Fig. 9). The key factor is the radius of the ZOI, which should at least correspond to the LVC size (3–5 trabeculae) while the weight function only plays a secondary role.

The magnitude of the external load regulates mechanical stimulation transferred from the implant to the surrounding tissue, and a study of the results' sensitivity to different load levels underlines the stimulation limits above which harmful effects are dominant. Indeed, the results are very sensitive to the load magnitude (Fig. 10) and evolve in a complex non-linear manner. The range of forces generating a positive effect on integration (i.e. augmentation of peri-implant density and improved implant stability) is found to be relatively narrow for the present experiment. Indeed, with 3.3 N bone reaction is quite limited while at 5 N the optimum is already reached. Higher loads provoke larger increases of BMD associated with dangerous peri-implant bone loss due to overloading (Fig. 11). Interestingly, the results spread increases significantly with load due to the difference between specimens. As a consequence, it can be postulated that the maximum forces to which each individual can adapt depends on specimen-specific features such as their initial bone structure, and therefore the results of this sensitivity study highlight the need to adopt a specimen specific approach to study critical overloading.

Moreover, the performed parametric studies allow establishing a ranking of the modeling parameters based on their effects on the inter-implant strain and maximum BMD variation (Fig. 13). Three categories are identified and can be adopted to optimize similar approaches:

- *Critical parameters*: the load overestimation and the absence of ZOI. They provoke more than 100% variation of both inter-implant strain and BMD in ROIs. If these parameters are not controlled or not implemented, the numerical predictions can become totally inconsistent. The ZOI should be set at least equal to 3–5 inter-trabecular spacing to avoid spurious mesh dependent effects. If critical loads are of interest, results extrapolated from populations or an average specimen can be imprecise. In this case a specimen specific approach is recommended.
- *Important parameters*: the adaptation thresholds, the piecewise law formulation with a plateau, the load underestimation and the ZOI radius overestimation. An ambiguous implementation of these parameters does not lead to unstable solutions, however the results are indeed inaccurate (between 10 and 100% error). At least, the bone adaptation threshold should be identified from physiological conditions and linear or quadratic adaptation law be implemented as a first option.
- *Negligible parameters*: the type of formulation (quadratic or linear adaptation law) and the type of decay function in the ZOI. These perturbations scarcely affect the predictions, and can be chosen arbitrarily.

In conclusion, among the different modeling hypothesis investigated here to predict peri-implant bone adaptation at the continuum level, a model formulation based on octahedral shear strain stimulus, a linear or quadratic evolution law and a ZOI equal to 3–5 inter-trabecular spacing is highly recommended based on the theoretical consistency considerations described in this work. The use of an histogram analysis of the stimuli in physiological loading conditions is also shown to provide a sound basis for the determination of the LZ bounds and for the selection of robust adaptation stimulus variable.

However, it is important to remind that this work is based on a phenomenological description of the bone adaptation at the continuum length scale which is at least two to three hierarchical levels above the cellular levels. The above recommendations conclusions should thus not be considered as hints on how bone physiology and mechano-transduction actually works at a smaller scale where the actual biophysical processes take place.

Finally, it should be noted that the proposed bone adaptation method has been successfully applied and compared to experimental data, as described in the works by Piccinini et al. [31] and

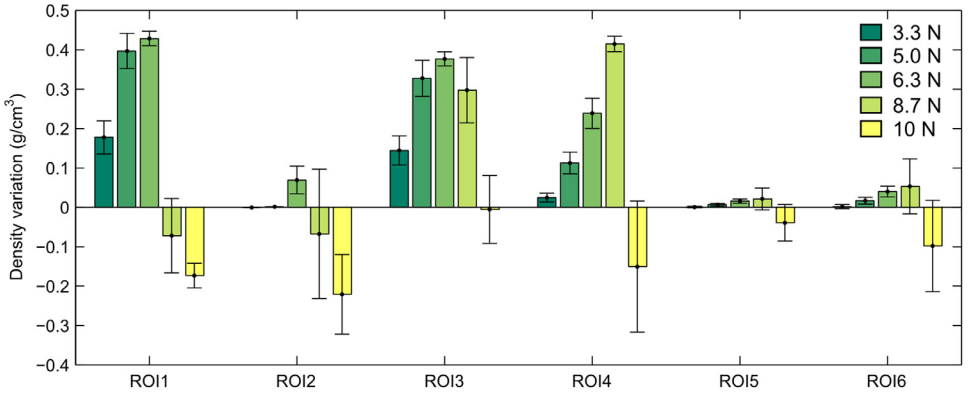

Fig. 12. Density in ROIs sensitivity to the external load magnitude. Mean values and SEM are represented.

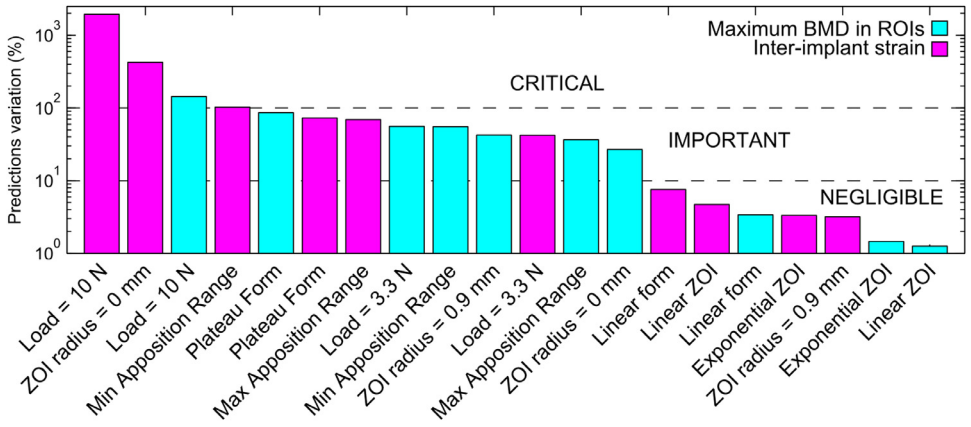

Fig. 13. Ranking of the perturbations analyzed by sensitivity studies. The variations are computed with respect to the results obtained with nominal settings (Table 1).

Piccinini [32]. The proposed model has shown consistent prediction with respect to the experimental observations in terms of BMD evolution and inter-implant strain evolution and was able to capture at least partially the specimen-specific response within a group. However, the physiological relevance of the above recommendations still need to be established for other experimental conditions.

Funding and Ethical Approvement

This work was partially funded by Swiss National Science Foundations (SNF) project 315230-127612 and internal funding from EPFL and UNIGE. All animal experiments were approved by the University of Geneva animal rights committee and supervised by the local veterinary board in accordance to Swiss regulations.

Conflict of interest

No conflict of interest.

Acknowledgments

Mrs. Severine Clement and Mrs. Isabelle Badoud are gratefully acknowledged for their work on experiments. This work was partially funded by Swiss National Science Foundations (SNF) project 315230-127612.

References

[1] Frost HM. Bone 'mass' and the 'mechanostat': a proposal. Anat Rec 1987;219:1–9.
[2] Huiskes R, Weinans H, Grootenboer HJ, Dalstra M, Fudala B, Slooff TJ. Adaptive bone-remodeling theory applied to prosthetic-design analysis. J Biomech 1987;20:1135–50.
[3] Mullender MG, Huiskes R. Proposal for the regulatory mechanism of Wolff's law. J Orthop Res 1995;13:503–12.
[4] Chou HY, Jagodnik JJ, Müftü S. Predictions of bone remodeling around dental implant systems. J Biomech 2008;41:1365–73.
[5] Mellal A, Wiskott HWA, Botsis J, Scherrer SS, Belser UC. Stimulating effect of implant loading on surrounding bone. Comparison of three numerical models and validation by in vivo data. Clin Oral Implant Res 2004;15:239–48.
[6] Reina JM, García-Aznar JM, Domínguez J, Doblaré M. Numerical estimation of bone density and elastic constants distribution in a human mandible. J Biomech 2007;40:828–36.
[7] Hoshaw SJ, Brunski JB, Cochran GVB, Higuchi KW. Theories of Bone Modeling and Remodeling in Response to Mechanical Usage: Experimental Investigation of an In Vivo Bone-Implant Interface. In: Goldstein SA, editor. 1990 Advances in Bioengineering. ASME, NY; 1990. p. 391–4.
[8] Qian J, Wennerberg A, Albrektsson T. Reasons for marginal bone loss around oral implants. Clin Implant Dent Relat Res 2012;14:792–807.
[9] Cox LGE, Van Rietbergen B, Van Donkelaar CC, Ito K. Analysis of bone architecture sensitivity for changes in mechanical loading, cellular activity, mechanotransduction, and tissue properties. Biomech Model Mechanobiol 2011;10:701–12.
[10] Weinans H, Huiskes R, Grootenboer HJ. The behavior of adaptive bone-remodeling simulation models. J Biomech 1992;25:1425–41.
[11] Beaupré GS, Orr TE, Carter DR. An approach for time-dependent bone modeling and remodeling - theoretical development. J Orthop Res 1990;8:651–61.
[12] Carter DR, Orr TE, Fyhrie DP. Relationships between loading history and femoral cancellous bone architecture. J Biomech 1989;22:231–44.
[13] Terrier A, Rakotomanana RL, Ramaniraka AN, Leyvraz PF. Adaptation models of anisotropic bone. Comput Methods Biomech Biomed Eng. 1997;1:47–59.
[14] Terrier A, Miyagaki J, Fujie H, Hayashi K, Rakotomanana L. Delay of intracortical bone remodelling following a stress change: a theoretical and experimental study. Clin Biomech 2005;20:998–1006.
[15] McNamara LM, Prendergast PJ. Bone remodelling algorithms incorporating both strain and microdamage stimuli. J Biomech 2007;40:1381–91.
[16] Li J, Li H, Shi L, Fok ASL, Ucer C, Devlin H, et al. A mathematical model for simulating the bone remodeling process under mechanical stimulus. Dent Mater 2007;23:1073–8.

[17] Crupi V, Guglielmino E, La Rosa G, Vander Sloten J, Van Oosterwyck H. Numerical analysis of bone adaptation around an oral implant due to overload stress. Proc Inst Mech Eng Part H J Eng Med 2004;218:407–15.
[18] Turner CH, Forwood MR, Otter MW. Mechanotransduction in bone: do bone cells act as sensors of fluid flow? FASEB J 1994;8:875–8.
[19] Schulte FA, Zwahlen A, Lambers FM, Kuhn G, Ruffoni D, Betts D, et al. Strain-adaptive in silico modeling of bone adaptation - A computer simulation validated by in vivo micro-computed tomography data. Bone 2013;52:485–92.
[20] Kumar NC, Jasiuk I, Dantzig J. Dissipation energy as a stimulus for cortical bone adaptation. J Mech Mater Struct 2011;6:303–19.
[21] Wiskott HWA, Cugnoni J, Scherrer SS, Ammann P, Botsis J, Belser UC. Bone reactions to controlled loading of endosseous implants: a pilot study. Clin Oral Implant Res 2008;19:1093–102.
[22] Wiskott HWA, Bonhote P, Cugnoni J, Durual S, Zacchetti G, Botsis J, et al. Implementation of the "loaded implant" model in the rat using a miniaturized setup - description of the method and first results. Clin Oral Implant Res 2011;23(12):1352–9.
[23] Zacchetti G, Wiskott A, Cugnoni J, Botsis J, Ammann P. External mechanical microstimuli modulate the osseointegration of titanium implants in rat tibiae. BioMed Res Int 2013:1–9 Article id: 234093.
[24] Piccinini M, Cugnoni J, Botsis J, Zacchetti G, Ammann P, Wiskott A Factors affecting subject-specific finite element models of implant-fitted rat bone specimens: Critical analysis of a technical protocol. Comput Methods Biomech Biomed Eng 2012;17(13):1403–17.
[25] Cory E, Nazarian A, Entezari V, Vartanians V, Müller R, Snyder BD. Compressive axial mechanical properties of rat bone as functions of bone volume fraction, apparent density and micro-ct based mineral density. J Biomech 2010;43:953–60.
[26] Piccinini M, Cugnoni J, Botsis J, Ammann P, Wiskott A. Influence of gait loads on implant integration in rat tibiae: experimental and numerical analysis. J Biomech 2014;47:3255–63.
[27] Lacroix D, Prendergast PJ. A mechano-regulation model for tissue differentiation during fracture healing: analysis of gap size and loading. J Biomech 2002;35:1163–71.
[28] Prendergast PJ, Huiskes R, Søballe K. Biophysical stimuli on cells during tissue differentiation at implant interfaces. J Biomech 1997;30:539–48.
[29] Van Rietbergen B, Huiskes R, Weinans H, Sumner DR, Turner TM, Galante JO. The mechanism of bone remodeling and resorption around press-fitted tha stems. J Biomech 1993;26:369–82.
[30] Harrigan TPJM, Mann RW, Harris WH. Limitations of the continuum assumption in cancellous bone. J Biomech 1988;21:269–75.
[31] Piccinini M, Cugnoni J, Botsis J, Ammann P, Wiskott A. Peri-implant bone adaptations to overloading in rat tibiae: experimental investigations and numerical predictions. Clin Oral Implant Res 2016. doi:10.1111/clr.12760.
[32] Piccinini M. Prediction of peri-implant bone adaptation to mechanical environments - theoretical developments and experimental validation, Ph.D. thesis, DOI: 10.5075/epfl-thesis-6273, URL: http://infoscience.epfl.ch/record/200508: EPFL; 2014.